POLITECNICO DI TORINO
Repository ISTITUZIONALE

Empowering the Tracking Performance of LEO-Based Positioning By Means of Meta-Signals

Original
Empowering the Tracking Performance of LEO-Based Positioning By Means of Meta-Signals / Nardin, Andrea; Dovis, Fabio; Fraire, Juan A.. - In: IEEE JOURNAL OF RADIO FREQUENCY IDENTIFICATION. - ISSN 2469-7281. - ELETTRONICO. - 5:3(2021), pp. 244-253. [10.1109/jrfid.2021.3077082]

Availability:
This version is available at: 11583/2902192 since: 2021-11-24T15:55:59Z

Publisher:
IEEE

Published
DOI:10.1109/jrfid.2021.3077082

Terms of use:

This article is made available under terms and conditions as specified in the corresponding bibliographic description in the repository

Publisher copyright
IEEE postprint/Author's Accepted Manuscript

©2021 IEEE. Personal use of this material is permitted. Permission from IEEE must be obtained for all other uses, in any current or future media, including reprinting/republishing this material for advertising or promotional purposes, creating new collecting works, for resale or lists, or reuse of any copyrighted component of this work in other works.

(Article begins on next page)

25 April 2024

Empowering the Tracking Performance of LEO-Based Positioning by Means of Meta-Signals

Andrea Nardin, *Student Member, IEEE*, Fabio Dovis, *Member, IEEE*, and Juan A. Fraire, *Senior Member, IEEE*

***Abstract*—Global Navigation Satellite Systems (GNSSs) are the most widespread technology for Position Navigation and Timing (PNT). They have been traditionally deployed exploiting Medium Earth Orbit (MEO) or Geosynchronous Orbit (GSO) satellites. To meet future demands and overcome MEO and GSO limitations, GNSSs based on Low Earth Orbit (LEO) constellations have been investigated as a radical system change. Although characterized by a higher Doppler effect, a PNT service supplied by LEO satellites can provide received signals that are about 30 dB stronger. Moreover, broadband LEO constellations and the forthcoming mega-constellations can be exploited to deliver a piggybacked PNT service. With this cost-effective solution, a PNT service might be subject to substantial bandwidth limitations. A narrowband implementation of the so-called meta-signal approach in GNSS receivers, namely Virtual Wideband (VWB), can tolerate harsh Doppler conditions while reducing the processed bandwidth. It is thus suited to a secondary PNT service delivered by LEO satellites. The aim of this work is to show the applicability of the VWB architecture to signals provided by a piggybacked PNT service, hosted on a mega-constellation. Through this case study we demonstrate the capability of this implementation to bear high Doppler conditions while empowering the potential of LEO PNT.**

***Index Terms*—Amazon Kuiper, DLL, GNSS, LEO PNT, mega-constellations, meta-signals, tracking.**

I. Introduction

GLOBAL Navigation Satellite Systems (GNSSs) are by far the most widespread technology for Position Navigation and Timing (PNT). They have been traditionally deployed exploiting Medium Earth Orbit (MEO) or Geosynchronous Orbit (GSO) satellite constellations. However, upcoming PNT applications are going to have challenging requirements and a radical system change might be needed to satisfy those demands.

Global macro-trends are going to drive the use of GNSS by industries and individuals demanding higher PNT accuracy and security [1]. However, signals' low power and limited bandwidth are intrinsic characteristics of current GNSSs that bound the achievable accuracy and threaten the robustness to intentional (jamming) and unintentional interference [2]. MEO and GSO GNSS signals are indeed subject to a strong free-space loss due to their long distance from Earth and they are all transmitted in the overcrowded L band, where bandwidth availability is scarce [2].

To meet future demands and overcome limitations, GNSSs based on Low Earth Orbit (LEO) constellations have been investigated as a radical system change. Although operating in a high Doppler effect scenario, a PNT service based on LEO satellites would offer a 30 dB smaller zenith path loss w.r.t. transmissions from MEO satellites [3]. Proposals for dedicated LEO GNSS constellations exist [3], but a promising approach relies on exploiting global Internet broadband constellations for PNT services [4]–[6]. The Iridium constellation is already providing a *hosted* PNT service [6] and new possibilities are foreseen thanks to companies like Amazon, Telesat, and SpaceX, which are deploying the so-called *mega-constellations* to provide global broadband Internet [3]. Nonetheless, a PNT service must provision its users with satellites' orbital and clock data. In a LEO framework, when a timely provision of such navigation data cannot be continuously guaranteed, complementary state estimation methods can be exploited [7], [8]. However, a discussion on navigation data dissemination for LEO PNT is out of the scope of this work.

The potential of a hosted PNT payload on LEO constellations has been analyzed in [4], [5] addressing dedicated PNT hardware on board. One step further is the *fused* approach, where existing broadband service resources (e.g., clocks, antennas, spectrum) are simultaneously exploited for PNT, providing a cost effective solution without reducing performance [9]. Major players for broadband mega-constellations are planning to transmit over sparsely occupied frequency bands (Ka, Ku, K, V bands) [3], potentially favoring a larger PNT-dedicated bandwidth w.r.t. traditional L-band GNSS. However, despite the bandwidth availability, a fused solution will be subject to resource limitations that depend on its commercial value with respect to the primary broadband service and spectral resources are no exception.

High Doppler and an economical use of bandwidth are not the only drawbacks of fused LEO PNT solutions. Although there are potentially many satellites flying by simultaneously over a single spot, LEO broadband constellations are mainly designed to have only one satellite serving a cell at any given time. Nonetheless the radio visibility of only a single PNT

Manuscript received January 15, 2021; revised March 12, 2021; accepted April 19, 2021. Date of publication May 3, 2021; date of current version August 27, 2021. *(Corresponding author: Andrea Nardin.)*

Andrea Nardin and Fabio Dovis are with the Department of Electronics and Telecommunications, Politecnico di Torino, 10124 Turin, Italy (e-mail: andrea.nardin@polito.it; fabio.dovis@polito.it).

Juan A. Fraire is with the Université de Lyon, Inria, INSA Lyon, CITI, 69621 Villeurbanne, France, also with the CONICET, Universidad Nacional de Córdoba, 5000 Córdoba, Argentina, and also with the Department of Dependable Systems and Software, Saarland University (Saarland Informatics Campus), 66123 Saarbrücken, Germany.

Digital Object Identifier 10.1109/JRFID.2021.3077082

This work is licensed under a Creative Commons Attribution 4.0 License. For more information, see https://creativecommons.org/licenses/by/4.0/

signal essentially prevents single-epoch pseudorange positioning. A strategy to overcome this problem is provided in [9]. According to the authors, PNT bursts can be directed towards neighboring cells for a fraction of the downlink communication time, causing a commercial loss for the primary service, whose sustainability can be calculated.

The introduction of *meta-signals* in the GNSS literature [10], [11] has brought a new receiver signal processing strategy, which is particularly effective in terms of available bandwidth exploitation. It allows to increase the positioning accuracy of a set of PNT signals, taking advantage of their frequency separation [12]. However, a wideband processing strategy might be critical when signals are affected by severe Doppler since a wideband signal is interested by a broader range of Doppler frequency shifts.

A more flexible implementation of the meta-signal concept has been presented in [13], overcoming the constrained distance between carrier frequencies. This approach leverages meta-signals by jointly processing PNT narrowband signals that may even share the same bandwidth, thus building a *Virtual Wideband* (VWB) signal. A VWB processing strategy is more effective when addressing a secondary PNT service, where a severely limited band occupation might be an essential requirement. Moreover it can tolerate harsh Doppler conditions thanks to its narrowband implementation.

The aim of this work is to show the applicability of a VWB meta-signal receiver architecture on signals provided through a fused LEO PNT service. We demonstrate the capability of this implementation to bear high Doppler conditions while empowering the potential of LEO PNT. Amazon's mega-constellation project Kuiper [14] is taken here as a sample candidate for a hypothetical fused LEO PNT service, by relying on the technical data in [15]. Thanks to a Software Defined Network approach, the high level of flexibility provided by its payload [15] makes it a good candidate for a fused service. The constellation comprises three orbital shells at as many different altitudes (590, 610, and 630 km). One satellite per orbital shell has been simulated along with atmospheric conditions to extract realistic Doppler profiles and C/N_0 values for three reference locations on Earth (low, intermediate and high Doppler conditions). A signal generator has been used to generate two BPSK-modulated LEO PNT signals consistent with the simulated Doppler characteristics and C/N_0 values. The signals are then jointly processed in a VWB fashion through a GNSS software receiver. A previous analysis focused on the initial service constellation [16] has been extended in this work to cover all the orbital shells. Such a comprehensive study enables a performance comparison among orbital altitudes. The outcome is non-trivial since, transmitting equipment being equal, satellites at lower orbital altitudes trade less favorable Doppler conditions with stronger received signals on Earth and vice versa.

The rest of the paper is organized as follows. Section II will introduce the meta-signals and the VWB approach. The satellite data acquisition and the signal generation process are described in detail in Section III along with the software receiver implementation. Results are then discussed in Section IV and conclusions are drawn in Section V.

II. The Meta-Signal Concept

The meta-signal processing (MSP) approach introduced in [10] is based on the well-known relationship between the Gabor bandwidth and the Cramér-Rao Lower Bound of the code thermal noise in a Delay-locked Loop (DLL) [2]:

$$\sigma^2_{DLL,CRLB} = \frac{B_n}{C/N_0 4\pi^2 \int_{-\infty}^{+\infty} f^2 G_s(f) df}. \tag{1}$$

In (1) B_n is the DLL bandwidth and C/N_0 and G_s are respectively the carrier-to-noise-density ratio and the normalized power spectral density of the processed signal. The term

$$B_{GB} = \sqrt{\int_{-\infty}^{+\infty} f^2 G_s(f) df} \tag{2}$$

is indeed the Gabor bandwidth and it is directly related to the code delay estimation precision as they both increase according to (1). Since any GNSS receiver's working principle is based on the estimation of the time-of-flight of a signal, the code delay estimation is in turn directly connected to the quality of the position estimation.

This concept motivated the definition of a wideband processing strategy that aims at maximizing the Gabor bandwidth of the processed signal by jointly tracking two frequency-separated PNT channels as a single wideband channel [11]. The channels are thus at the edges of the power spectral density of the processed signal, resulting in an increased Gabor bandwidth. The net result is a superposition of the frequency-shifted versions of the original channels, which is processed within the baseband DSP chain. By looking it from a different perspective, this "meta-signal" presents an Auto-correlation Function (ACF) which is essentially modulated by a carrier [11]. As reported in Fig. 1, such an ACF has a narrower main peak, a property directly related to a code tracking performance improvement [17]. The ACF exhibits also an increased peak ambiguity, whose severeness depends on the frequency separation between the combined channels. Therefore, as long as we are able to tolerate the ambiguity, it is possible to exploit the increased sharpness to reduce the correlator Early-minus-Late (E-L) spacing, while keeping the gap between Prompt (P) and Early (E) or Late (L) correlator outputs constant (see Fig. 1). This means that we can tolerate the same amount of noise (thanks to the gap) while attaining an improved code tracking jitter (thanks to E-L spacing reduction) [18].

A. The Virtual Wideband Implementation

An additional approach to MSP has been introduced in [13]. According to this architecture, two narrowband signals are received by a front-end stage and fed to the processing chain as baseband signals. Within the tracking loop, these signals are up-converted to two opposite frequencies, thus introducing a frequency separation between them. The signals are then correlated with local replicas and combined at a post-correlator level. Through this method an equivalent VWB signal is processed in the receiver at the cost of a complexity increase.

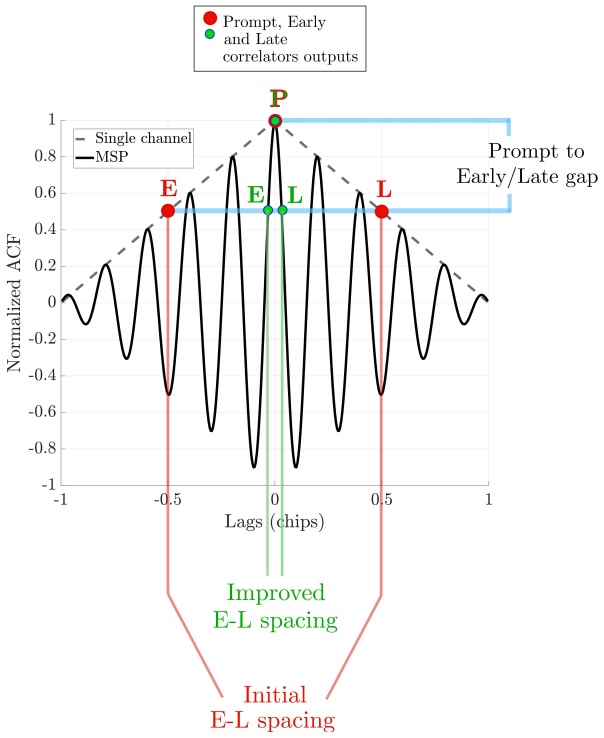

Fig. 1. Autocorrelation function of a single BPSK signal and a meta-signal made by two BPSK channels.

Nonetheless, the resulting flexibility overcomes two major limitations of standard MSP. First, the separate narrowband band processing of the two PNT channels enables a two-stages peak ambiguity resolution scheme. The narrowband channels are initially processed independently, in a standard *single-channel* (SC) processing, to solve the peak ambiguity. A closed loop implementation of this stage is shown in Fig. 2, focusing on one of the two channels and highlighting the spectral characteristics of the signals throughout the loop. The residual carrier and doppler frequency shift are removed from the intermediate frequency (IF) signal $y_{L,IF}(t)$ to obtain the baseband signal $s_L(t)$, which is then processed by the DLL. The subsequent phase (Fig. 3) enables a channel combination where the two baseband signals $s_L(t)$ and $s_R(t)$ are shifted in frequency to $-f_m/2$ and $+f_m/2$ respectively. The resulting signals $x_L(t)$ and $x_R(t)$ are then jointly processed within the DLL in a meta-signal fashion, according to the scheme in Fig. 4. This MSP phase is triggered only once the receiver is locked over the main peak. Referring again to Fig. 1, by processing a single BPSK channel through the loop in Fig. 2, we are able to align the DLL consistently with the dashed grey ACF in the diagram. If the main peak of this curve is estimated with sufficiently high precision, the receiver is able to lock over the main peak of the meta-signal's ACF. The ambiguity is solved by means of the narrowband signals while the improved accuracy is brought by the VWB blocks, through the higher-frequency signals, similarly to a fixed-tone ranging system [13], [19].

The second advantage of this flexible architecture is that it allows to adjust the frequency separation of the channels

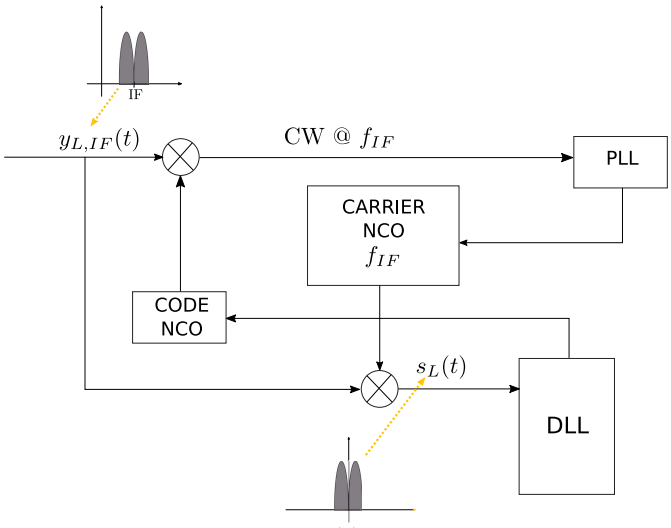

Fig. 2. Single channel tracking (first stage).

within the DSP chain. Indeed, the value of f_m is a free parameter of the system and can be freely set as long as the Nyquist rate is fulfilled and the resulting peak ambiguity is tolerated. It is therefore possible to further enhance the Gabor bandwidth for channels that have a small or even null frequency separation in the Signal-In-Space. This might be a substantial advantage in the LEO PNT framework, where a small carrier frequency difference results in a significant variation of Doppler frequency shift. Furthermore, it is even more appealing for fused solutions, where an economical use of spectral resources is of primary importance.

III. Signal Generation and Processing

In this Section we describe the data collection process that led to the PNT signals generation. Doppler shift profiles and power levels extracted from the constellation simulator have been fed to the binary signal generator to simulate the received PNT signals. A description of the receiver configuration employed to track those signals is also provided.

A. Reference Constellation Scenario

In order to analyze the applicability of VWB PNT in upcoming mega-constellations, we consider, as a case study, the Amazon's mega-constellation project Kuiper. According to [15], Kuiper fleet will be composed of 3236 LEO satellites providing high-speed and low-latency satellite broadband services. Satellites will be deployed in three "shells" at different altitudes, over circular orbits (see Table I). In a previous work [16], we focused the analysis on the 630 km orbital shell, the first to be deployed [15], leveraging existing Amazon's terrestrial networking infrastructure on the ground segment side. In this work, we are investigating all the orbital altitudes planned for the upcoming constellation. We are therefore including in the case study those satellites that are closer to Earth, i.e., they are subject to stronger Doppler shifts, but better C/N_0 levels.

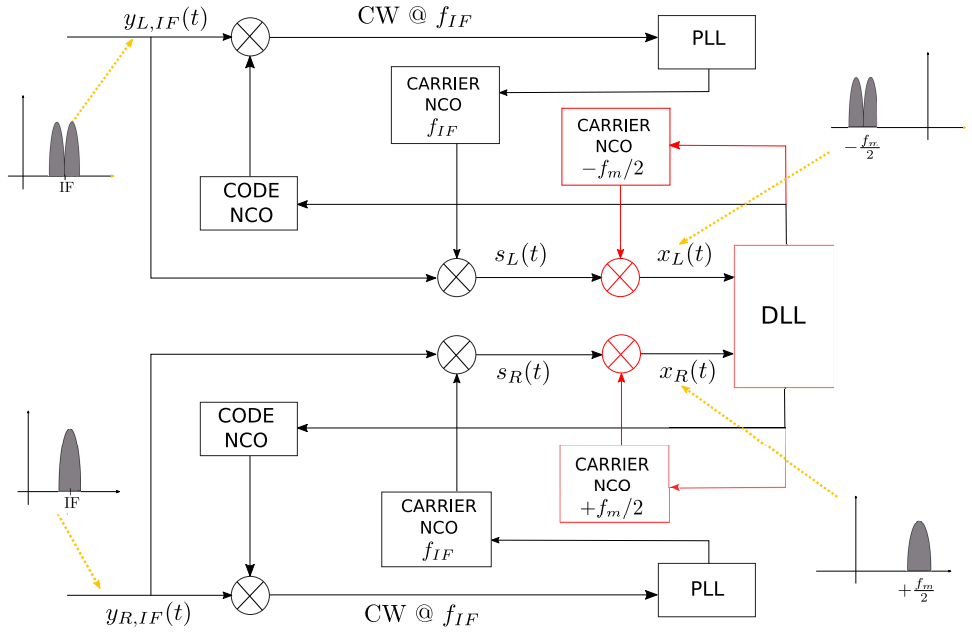

Fig. 3. Virtual Wideband tracking implementation (second stage).

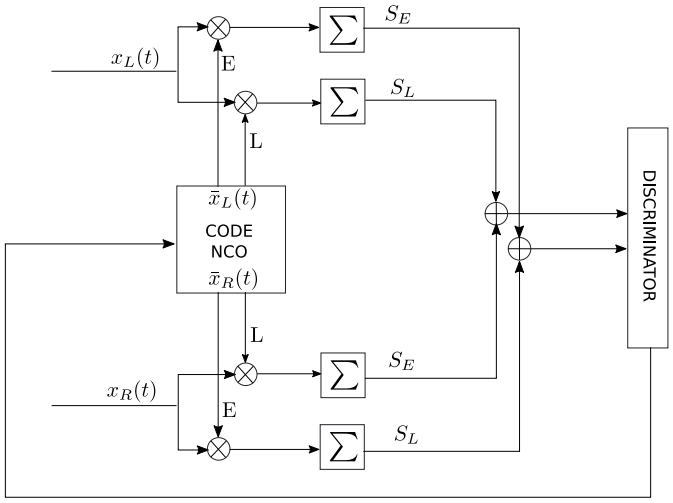

Fig. 4. Meta-signal DLL implementation.

TABLE I
AMAZON'S KUIPER CONSTELLATION PARAMETERS

Altitude	Inclination	Planes	Sats/Plane	Satellites
630 km	51.9 deg	34	34	1156
610 km	42 deg	36	36	1296
590 km	33 deg	28	28	784

The Kuiper constellation was simulated on AGI's Systems Toolkit (STK) software. Table II provides the specific details of the evaluated scenario. The transmitter's beamwidth and EIRP can be found in the documentation attached to the FCC application [15]. The receiver's antenna gain-to-noise-temperature (G/T) has been set assuming a uniform 3 dB gain in the upper hemisphere and a noise power density $N_0 = -204.4$ dBW-Hz [20]. Three reference points $N1$, $N2$ and $N3$ have been deployed on the center, mid-range and far-range of one of the passing by satellite's footprint (see Fig. 5), within the boundaries of initial service coverage latitudes [15]. Two additional satellites have been simulated in the 610 km and 590 km orbits along the zenith direction of point $N1$. In this way, we obtained three satellite passes, comprising low, mid and high peak elevation from the reference points. We are thus able to evaluate the access over these ground points for each of the selected satellites. The evolution of the Doppler frequency shift (see Fig. 6) and C/N_0 values experienced by users at these points of interest were exported for two adjacent frequency channels along the satellite pass.

TABLE II
STK SCENARIO PARAMETERS

Parameter	Value
Pass date	1 Jan 2020 00:03:00.00
Tx Beamwidth	48.2 deg
Tx Frequency	19.298 GHz and 19.295 GHz
Tx EIRP	43.1 dBW
Rx G/T	-21.19 dB/K
Modulation	BPSK
Data Rate	50 b/sec
CDMA spread	20460 chips/bit
Bandwidth	2.046 MHz
Atmospheric impairments	Cloud and fog (ITU-R P840-6) Tropo. scintillation (ITU-R P618-12) Ionospheric fading (ITU-R P531-13)

B. PNT Signals Generation

The Doppler profiles extracted from the simulated satellites passing over the three reference positions and the average C/N_0 levels were used to shape the GNSS-like signals generated by a digital signal generator. To this purpose, a GNSS signal generator named N-FUELS (FUll Educational Library of Signals for Navigation) [21] and based on MATLAB was

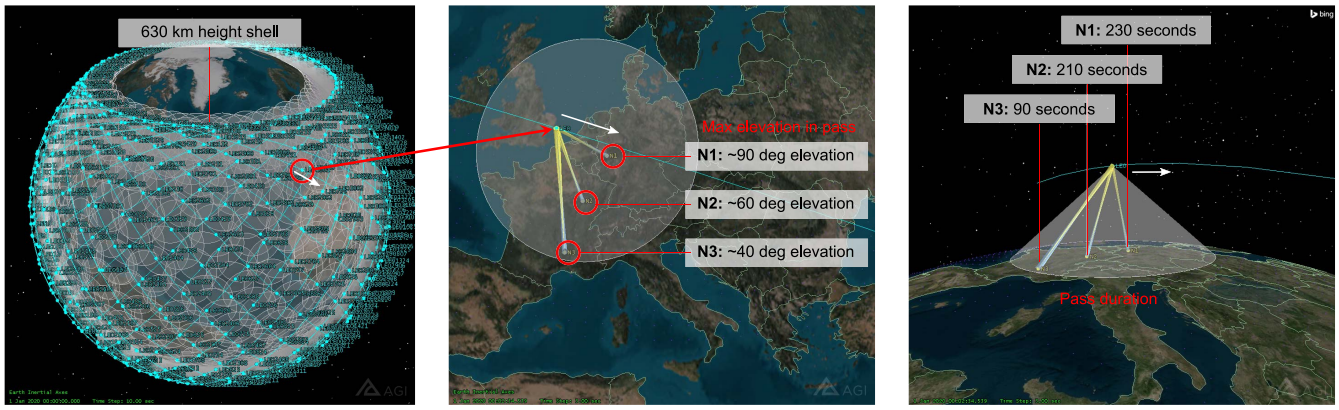

Fig. 5. Highest orbital shell of Kuiper constellation and sample pass with reference points N1, N2 and N3.

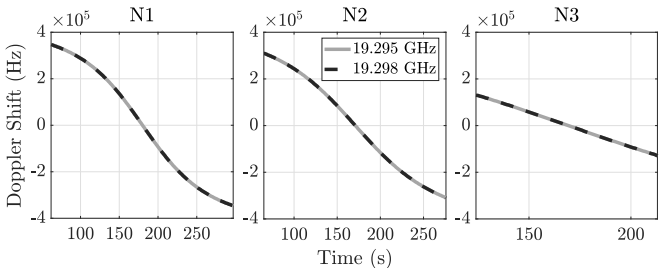

(a) Orbital altitude 630 km

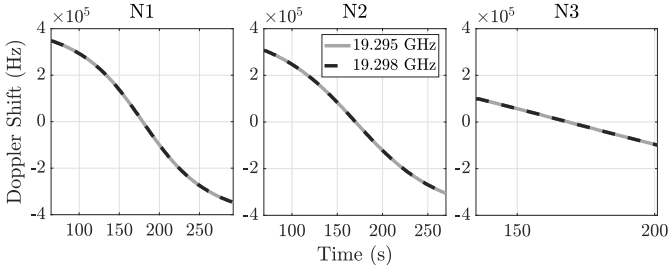

(b) Orbital altitude 610 km

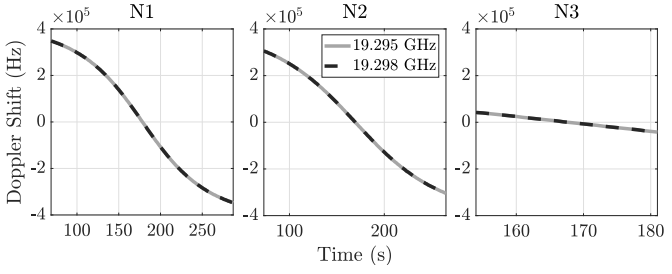

(c) Orbital altitude 590 km

Fig. 6. Doppler profiles at reference points N1, N2 and N3.

employed. N-FUELS outputs digital baseband signals, simulating the behavior of a user-defined RF front-end. It has been fed with the Doppler profiles sampled at 1 Hz.

The generated signals are BPSK-modulated with a chiprate of 1.023 MHz, often referred to as BPSK(1) in GNSS literature [22]. The purpose of using simple GNSS signals like the GPS L1 C/A signal [23] is twofold. On the one hand, we want to use a plain GNSS signal that does not add additional complexity to the receiver architecture. In this way we can steer the analysis to the tracking in LEO high-dynamics conditions and to the benefits of our proposed VWB architecture. On the other hand, since we are considering a fused secondary service on a broadband satellite payload, we want to limit the bandwidth resources devoted to PNT.

TABLE III
SIGNAL GENERATOR COMMON PARAMETERS

Parameter	Value
Sampling Frequency	25 MHz
Intermediate Frequency	0 Hz
Binary signal type	int8
Quantization bits	7
Code delay	0.5 ms
Noise Density	-204.4 dBW-Hz

According to the documentation attached to the FCC application [15], Amazon Kuiper services will be delivered in the K_u, K and K_a bands. Supposing to host a PNT service on *user downlink beams*, the highest spectrum designation band during initial service deployment is a 500 MHz aggregated channel in the 18.8-19.3 GHz band. We chose to set the signal central frequencies in the highest available band in order to address a worst-case Doppler situation. Moreover, this condition would be also the most favorable for PNT from a theoretical point of view, since a higher carrier frequency has the potential to increase the estimation resolution [19].

Two PNT channels are necessary to build a meta-signal in the VWB receiver. To this end, we investigated the combination of one data channel and one pilot channel in two different arrangements, both commonplace in GNSSs signal plans:

- S1 two BPSK(1) channels over the same bandwidth at a central frequency $f_c = 19.298$ GHz. Channels' multiple access is provided through orthogonality of spreading codes. This arrangement is similar to E1B and E1C in Galileo [24];
- S2 two BPSK(1) channels on adjacent bands, centered at respectively f_c and $f_c' = 19.295$ GHz to accommodate a guard band in between.

The generation of the raw binary signals in N-FUELS is carried out according to the parameters in Tables III and IV, using constant C/N_0 levels based on the average values. The Doppler profiles (Fig. 6) obtained simulating the transmission

TABLE IV
AVERAGE C/N_0 AND RECEIVED POWER

Altitude	Parameter	Value		
		N1	N2	N3
630 km	Average C/N_0 (dB-Hz)	72.43	71.63	69.57
	Average Carrier power (dBW)	-134.98	-135.78	-137.84
610 km	Average C/N_0 (dB-Hz)	72.70	71.87	69.72
	Average Carrier power (dBW)	-134.71	-135.54	-137.69
590 km	Average C/N_0 (dB-Hz)	73.00	72.11	69.88
	Average Carrier power (dBW)	-134.41	-135.30	-137.53

TABLE V
SOFTWARE RECEIVER CONFIGURATION

Parameter	Value
Coherent integration time	2 ms
PLL order	3
E-L spacing	1 chip
MSP E-L spacing	0.025 chip
Tracking Lock Indicator threshold	0.8
Virtual frequency separation	18.414 MHz

of signals S1 and S2 in STK are loaded into the signal generator, which, after interpolation, apply them both on the carrier and on the spreading code. The net result is a set of realistic signals, that take into account the effect of Line-of-Sight (LOS) dynamics, the atmospheric effects (see Table II) and the presence of thermal noise at the receiver.

C. Receiver Processing Architecture

The binary signals have been processed through a GNSS software receiver based on MATLAB, which has been fine-tuned to properly track the LEO PNT signals of the Kuiper constellation. The configuration parameters are summarized in Table V.

To properly track the LOS dynamics of the LEO context, a third order PLL has been used. This type of PLL proved to be suitable to the broad range of Doppler conditions investigated, successfully following a stressing phase dynamics without leading to instability issues. It is worth noting that these kind of signals demand also a large PLL noise bandwidth and a large DLL noise bandwidth as well, if the latter is not taking advantage of a carrier aiding technique. The tracking loop is therefore generally less robust to thermal noise. However, the signals are also characterized by a C/N_0, which is much larger than commonplace GNSS values (around 45 dB-Hz [25]) and can counterbalance this drawback.

The tracking stage of the software receiver is a working VWB implementation of the closed-loop block schemes in Figs. 2 and 3. As described in Section II, the actual MSP stage is triggered once the tracking loop is locked. A tracking lock indicator as defined in [26] is exploited to start the MSP stage once the lock indicator value is above the threshold defined in Table V. The tracking lock indicator is defined as

$$PLI = \frac{I_P^2 - Q_P^2}{I_P^2 + Q_P^2} \tag{3}$$

where I_P and Q_P are respectively the in-phase and quadrature P correlator outputs, computed at each tracking loop iteration.

Once the MSP tracking loop is running, the E-L spacing is reduced to allow the DLL to take advantage of the enhanced gap between the P correlator and E or L correlator output (a consequence of the ACF peak sharpening). In order to get a fair comparison between SC processing and MSP, the nominal gap is left unaltered before and after the MSP triggering. The gap has been computed theoretically by considering the C/N_0 and the nominal ACFs of both the single BPSK(1) signal and the meta-signal (see Fig. 1), A spacing of 0.025 chip has been therefore calculated as corresponding to the original spacing of 1 chip.

IV. RESULTS

In this section we present and discuss the processing results provided by the MSP software receiver after tracking realistic LEO PNT signals as received by static users at the three reference locations. The two-stages architecture enables a straightforward comparison between SC processing and MSP performances by simply observing the outcome from, respectively, the first and the second stage. The main performance metrics considered are

- the *code error* (CE), as provided at the output of the DLL discriminator after a conversion in meters;
- the *code-rate error* (CRE), computed in chip/s.

CE and code-rate estimations have been observed within the DLL, first in the SC tracking stage and subsequently in the MSP tracking stage.

As stated in Section II, the capability of the DLL to successfully track the code delay of the incoming PNT signal is directly related to a correct estimation of the distance between the receiver and the satellite and, in turn, to an accurate positioning [18]. As a consequence, a less noisy CE leads to a more precise position estimation. In particular, within the DLL the CE is filtered through the loop filter to obtain the CRE. The code NCO in Fig. 4 is ultimately driven by the magnitude and sign of the estimated CRE value to seek a continuous alignment with the received signal and thus towards a lock on a correct code delay. The CRE has been estimated exploiting a noiseless signal. Such an ideal signal has been generated with identical characteristics and carrier power of the signal under test, but in the absence of thermal noise. The code-rate estimation is in fact subject to LOS dynamic stress since the code tracking loop is not smoothed by carrier aiding. Each code-rate estimation is thus still affected by the code Doppler, which has not been smoothed. The estimated code-rate of the noiseless signal is characterized by the code Doppler as well and it can be successfully used to de-trend the S1 and S2 code-rate estimations. The CRE is then computed by subtracting the estimated code-rate of the noiseless signal to the estimated code-rate of the signal under investigation. The net result is a measure of the estimation error caused by the presence of thermal noise within the signals.

The estimated errors in Fig. 7 were obtained at location N2, observing a satellite passage from the 610 km orbit. The

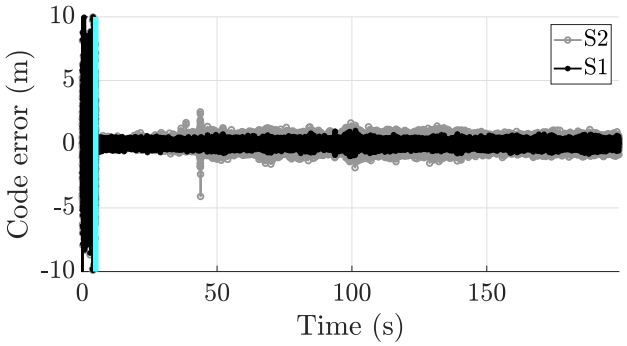

(a) Code error estimation

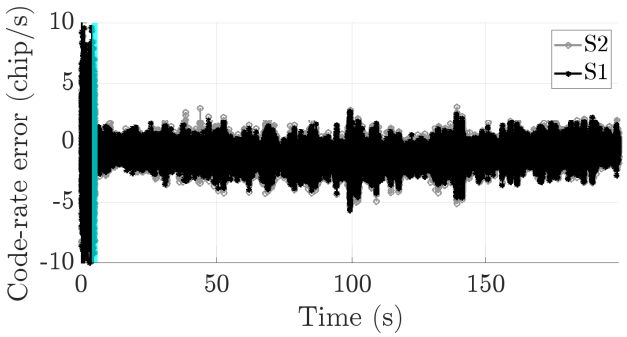

(b) Code-rate error estimation

Fig. 7. Code error and code-rate error for N2 reference location and 610 km orbital altitude. The cyan line highlights the transition from SC processing to MSP.

TABLE VI
RMSE OF CODE AND CODE-RATE ERROR AT 630 KM

	N1		N2		N3	
	S1	*S2*	*S1*	*S2*	*S1*	*S2*
SC stage CE (m)	2.97	2.97	3.38	3.38	4.29	4.29
MSP stage CE (m)	0.20	0.30	0.20	0.32	0.23	0.17
RMSE reduction (%)	93.2	90.0	94.1	90.7	94.5	96.0
SC stage CRE (chip/s)	3.15	3.15	3.61	3.61	4.65	4.65
MSP stage CRE (chip/s)	1.25	1.28	1.20	1.23	1.17	1.19
RMSE reduction (%)	60.2	59.3	66.9	65.8	74.7	74.4

TABLE VII
RMSE OF CODE AND CODE-RATE ERROR AT 610 KM

	N1		N2		N3	
	S1	*S2*	*S1*	*S2*	*S1*	*S2*
SC stage CE (m)	3.21	3.21	3.25	3.25	4.25	4.25
MSP stage CE (m)	0.21	0.29	0.20	0.32	0.24	0.16
RMSE reduction (%)	93.5	91.1	93.9	90.2	94.5	96.2
SC stage CRE (chip/s)	3.42	3.42	3.49	3.49	4.58	4.58
MSP stage CRE (chip/s)	1.29	1.31	1.23	1.26	1.23	1.22
RMSE reduction (%)	62.3	61.6	64.8	63.8	73.2	73.3

plots describe the DLL performance for both signal arrangements S1 and S2, highlighting the transition from the SC stage (prior to MSP triggering) to the MSP stage (indicated by the cyan vertical line). A great reduction of the error is clearly visible when the MSP loop is activated, both in terms of code and code-rate. A similar improvement is visible with all the considered reference locations and orbital altitudes, and for both signal arrangements. For the sake of brevity we do

TABLE VIII
RMSE OF CODE AND CODE-RATE ERROR AT 590 KM

	N1		N2		N3	
	S1	*S2*	*S1*	*S2*	*S1*	*S2*
SC stage CE (m)	2.83	2.83	3.22	3.23	4.01	4.01
MSP stage CE (m)	0.20	0.29	0.19	0.30	0.28	0.22
RMSE reduction (%)	92.8	89.9	94.0	90.7	93.0	94.6
SC stage CRE (chip/s)	3.02	3.02	3.44	3.45	4.31	4.31
MSP stage CRE (chip/s)	1.33	1.35	1.27	1.29	1.37	1.36
RMSE reduction (%)	56.1	55.4	63.3	62.5	68.1	68.4

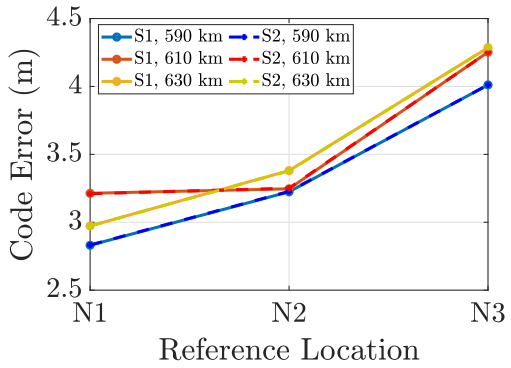

(a) Code error

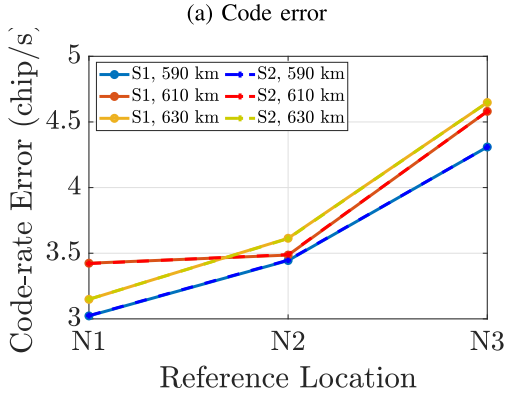

(b) Code-rate error

Fig. 8. Code error and code-rate error for the SC stage, as experienced at the three reference locations under test. (a) Code error (b) Code-rate error

not report all the time series plots in this paper. However, to efficiently compare all the eighteen experiments, we exploited the Root Mean Square Error (RMSE) as a comprehensive and aggregated metric.

The RMSEs were computed over DLL output data as those reported in Fig. 7. The resulting values are collected in Tables VI, VII, and VIII to ease the comparison. RMSEs are computed separately over the initial SC stage and the MSP stage. The RMSE of the SC stage is calculated by omitting the initial transient of the receiver's tracking loop, which is never below 0.5 s, as estimated by comparison with the noiseless processing outcomes. Nevertheless, the tracking lock indicator has been activated only after 5 s, to provide a meaningful statistic for the RMSE of the SC phase.

Looking at Tables VI, VII, and VIII, it is worth noting that for almost all the configurations S1 leads to a better estimation error when MSP is active. This is basically always true,

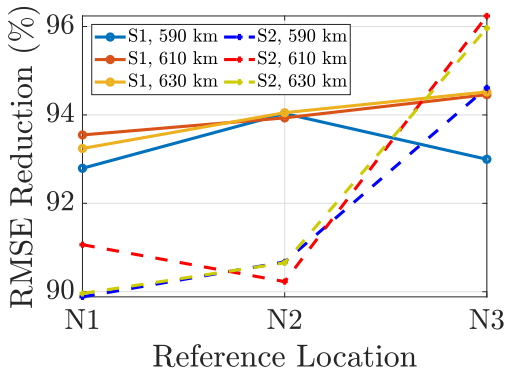

(a) RMSE reduction of code error

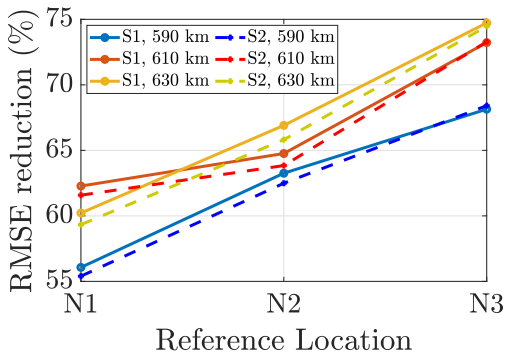

(b) RMSE reduction of code-rate error

Fig. 9. RMSE reduction between SC and MSP stages, as experienced at the three reference locations under test. (a) RMSE reduction of code error (b) RMSE reduction of code-rate error

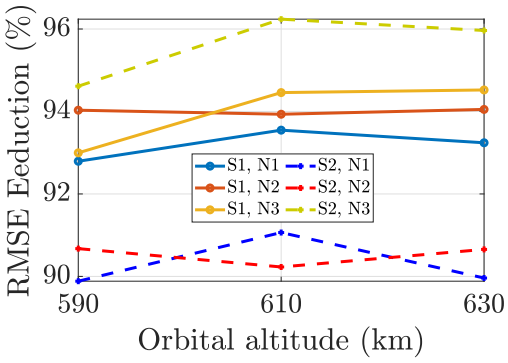

(a) RMSE reduction of code error

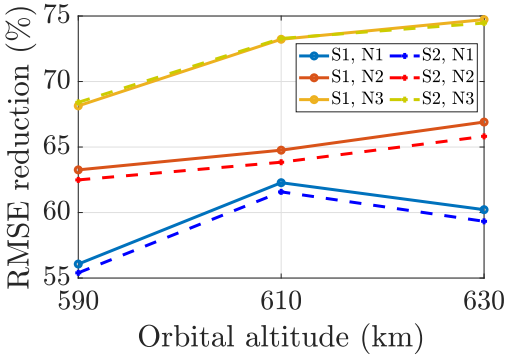

(b) RMSE reduction of code-rate error

Fig. 10. RMSE reduction between SC and MSP stages, as experienced at the three orbital altitudes of the Kuiper constellation.

exception made for the location N3. This reference point is characterized by a Doppler shift which spans between smaller values w.r.t. the other locations. Nonetheless this transition is characterized by a slower pace and, as a matter of fact, the configuration S2 benefits more than S1 from these favorable Doppler conditions. Indeed, the two channels in the S2 configuration are centered over adjacent but different carriers. They experience therefore a different Doppler shift. These two channels, jointly processed within the MSP receiver, are thus characterized by different frequencies. Although this difference is small (see Fig. 6), this is in principle a challenging condition for the tracking loop. The PLL loops within the MSP architecture must be in fact sufficiently independent to successfully track different carriers. As a result, less favorable Doppler conditions (such as those experienced at N1 and N2) are more challenging for S2, which is penalized w.r.t. S1. On the other hand, this configuration is advantageous where the Doppler shift is limited (as in N3), resulting in a RMSE that can even outperform other configurations, that are characterized by a larger C/N_0 (as reported in Table IV). Nonetheless, S1 and S2 give comparable RMSEs, meaning that through the VWB architecture it is possible to obtain almost the same code tracking performance of a signal (S2) that needs a bandwidth occupation which is at least doubled.

At the reference point N3, a GNSS receiver would experience the worst average C/N_0 (see Table IV). As highlighted by Fig. 8, the SC tracking stage is primarily affected by this signal deterioration. The reference point N3 is in fact the worst performing location in all configurations, both in terms of CE (Fig. 8(a)) and CRE (Fig. 8(b)). Despite this, the VWB architecture copes well with the weakening of received signals, providing, for N3, the highest RMSE reduction for almost all the configurations, as seen in Fig. 9. The RMSE reduction in Fig. 9, enabled by the MSP stage, exhibits an interesting trend if compared to Fig. 8. The performance improvement increases as the Doppler conditions become more favorable and the C/N_0 gets worse. Hence, when the satellite passage has a low elevation peak, and thus a desirable Doppler profile, the proposed technique provides a performance gain that is even more significant than the RMSE obtained when the average received power is almost doubled (as per location N1).

Analogous considerations can be drawn by comparing the different orbital shells composing the space segment of the Kuiper system. However, the signals transmitted from the three orbital altitudes are characterized by both a small variation of the received power (Table IV) and rather similar Doppler profiles (Fig. 6). As a consequence, no significant performance variation of the CE can be observed w.r.t. the orbital altitude, as highlighted by Fig. 10(a). Nonetheless, the improvement is generally larger for the 630 km orbit, whose signals are characterized by a less severe Doppler shift and a lower received power. This trend is especially visible regarding CRE estimation, as shown by Fig. 10(b).

According to the reported results, it is clear that the high dynamics conditions caused by a challenging Doppler shift

greatly impact the VWB architecture. This is a non-trivial outcome since the SC stage performance was found to be instead mainly driven by the received signal power. The technique, however, proved to be highly profitable in all the experiments, mitigating the severe LOS dynamic stress that characterizes LEO transmissions. Indeed, it is worth to point out that the RMSE reduction was always greater than 89.9% and 55.4% for CE and CRE estimation respectively, in all the tested configurations.

V. Conclusion

The LEO PNT approach has gained popularity in recent years as a way to overcome some of the existing GNSS shortcomings (e.g., low C/N_0). In this regard, a fused LEO PNT approach would offer a low-cost implementation of a PNT service at the price of a limited resource availability. In this framework, the VWB approach to meta-signals can leverage a limited signal bandwidth to improve the receiver capability to provide an accurate position estimation. In this paper we investigated the performance of the VWB architecture applied to LEO PNT signals. We simulated a fused PNT service hosted by Amazon Kuiper, the forthcoming broadband mega-constellation. Realistic signals transmitted from three different orbital altitudes and received in three different Earth locations were processed according to a VWB paradigm for meta-signals. In all the configurations, we tested two different signal arrangements, namely S1 and S2.

The analysis showed that the signal arrangement S2 is outperformed by S1 when the Doppler conditions are challenging. Therefore, being S1 also efficient in terms of bandwidth usage, it should be the preferred configuration in a LEO PNT framework. Moreover, the analysis focused on the comparison among different Earth locations and different orbital altitudes. The latter however, have a limited impact on the resulting performance, being characterized by a high similarity in terms of Doppler profile and received power. As a result, each of the planned orbital shell of the Kuiper space segment is potentially suitable for a LEO PNT service. On the other hand, the comparison among reference locations allowed to analyze the impact of non-negligible variations of Doppler effect intensity and C/N_0 levels. We found that in this framework the Doppler conditions are the main driver of the MSP performance, whereas the plain SC processing resulted primarily conditioned by the C/N_0 parameter. Nonetheless, the proposed technique resulted beneficial for all the configurations assessed, which are representative of the Kuiper case study and, more generally, of an envisioned fused LEO PNT service. For a receiver that can bear the increased complexity of the implementation, the meta-signal architecture has been proven an advantageous tracking scheme under high C/N_0 and large Doppler shifts, both peculiar conditions of LEO transmissions. Furthermore, the high signal to noise ratio allows to employ large PLL and DLL noise bandwidths, hence adapting the software receiver to the high Doppler stress. Nevertheless, a future analysis shall involve specific high-dynamics receivers, to further exploit the potential of a MSP architecture.

References

[1] *GNSS Market Report Issue 6*, Luxembourg City, Luxembourg, Eur. GNSS Agency, 2019.

[2] P. J. G. Teunissen and O. Montenbruck, *Springer Handbook of Global Navigation Satellite Systems*. Cham, Switzerland: Springer, 2017.

[3] T. G. R. Reid *et al.*, "Satellite navigation for the age of autonomy," in *Proc. IEEE/ION Position Location Navig. Symp. (PLANS)*, 2020, pp. 342–352.

[4] T. G. Reid, A. M. Neish, T. F. Walter, and P. K. Enge, "Leveraging commercial broadband LEO constellations for navigation," in *Proc. 29th Int. Techn. Meeting Satellite Div. Inst. Navig. (ION GNSS)*, 2016, pp. 2300–2314.

[5] T. G. R. Reid, A. M. Neish, T. Walter, and P. K. Enge, "Broadband LEO constellations for navigation," *Navigation*, vol. 65, no. 2, pp. 205–220, 2018. [Online]. Available: https://onlinelibrary.wiley.com/doi/abs/10.1002/navi.234

[6] G. Gutt, D. Lawrence, S. Cobb, and M. O'Connor, "Recent PNT improvements and test results based on low earth orbit satellites," in *Proc. Int. Techn. Meeting Inst. Navig.*, 2018, pp. 570–577.

[7] Z. Kassas, J. Morales, and J. Khalife, "New-age satellite-based navigation STAN: Simultaneous tracking and navigation with LEO satellite signals," *Inside GNSS Mag.*, vol. 14, no. 4, pp. 56–65, 2019.

[8] C. T. Ardito, J. J. Morales, J. Khalife, A. A. Abdallah, and Z. M. Kassas, "Performance evaluation of navigation using LEO satellite signals with periodically transmitted satellite positions," in *Proc. Int. Techn. Meeting Inst. Navig.*, 2019, pp. 306–318.

[9] P. A. Iannucci and T. E. Humphreys, "Economical fused LEO GNSS," in *Proc. IEEE/ION Position Location Navig. Symp. (PLANS)*, Portland, OR, USA, 2020, pp. 426–443.

[10] J.-L. Issler, M. Paonni, and B. Eissfeller, "Toward centimetric positioning thanks to L- and S-band GNSS and to meta-GNSS signals," in *Proc. 5th ESA Workshop Satellite Navig. Technol. Eur. Workshop GNSS Signals Signal Process. (NAVITEC)*, Noordwijk, The Netherlands, 2010, pp. 1–8.

[11] M. Paonni, J. T. Curran, M. Bavaro, and J. Fortuny-Guasch, "GNSS meta signals: Coherently composite processing of multiple GNSS signals," in *Proc. 27th Int. Techn. Meeting Satellite Div. Inst. Navig.*, Tampa, FL, USA, 2014, pp. 2592–2601.

[12] P. Das, L. Ortega, J. Vilá-Valls, F. Vincent, E. Chaumette, and L. Davain, "Performance limits of GNSS code-based precise positioning: GPS, Galileo & meta-signals," *Sensors*, vol. 20, no. 8, p. 2196, 2020. [Online]. Available: https://www.mdpi.com/1424-8220/20/8/2196

[13] A. Nardin, F. Dovis, and B. Motella, "Impact of non-idealities on GNSS meta-signals processing," in *Proc. Eur. Navig. Conf. (ENC)*, Dresden, Germany, Nov. 2020, pp. 1–8.

[14] C. Henry, *Amazon's Kuiper Constellation Gets FCC Approval*, SpaceNews, Alexandria, VA, USA, 2020. Accessed: Sep. 11, 2020. [Online]. Available: https://spacenews.com/amazons-kuiper-constellation-gets-fcc-approval

[15] *Application of Kuiper Systems LLC for Authority to Launch and Operate a Non-Geostationary Satellite Orbit System in Ka-Band Frequencies and Attachments*, Amazon, Seattle, WA, USA, 2019.

[16] A. Nardin, F. Dovis, and J. A. Fraire, "Empowering the tracking performance of LEO PNT by means of meta-signals," in *Proc. IEEE Int. Conf. Wireless Space Extreme Environ. (WiSEE)*, Vicenza, Italy, 2020, pp. 153–158.

[17] J. W. Betz, "The offset carrier modulation for GPS modernization," in *Proc. Nat. Techn. Meeting Inst. Navig.*, San Diego, CA, USA, 1999, pp. 639–648.

[18] E. Kaplan and C. Hegarty, *Understanding GPS: Principles and Applications*. Boston, MA, USA: Artech House, 2005.

[19] W. C. Lindsey and M. K. Simon, *Telecommunication Systems Engineering*. Englewood Cliffs, NJ, USA: Prentice-Hall, 1991.

[20] R. B. Langley, *GPS Receiver System Noise*, vol. 8, GPS World, Cleveland, OH, USA, 1997, pp. 40–45.

[21] E. Falletti, D. Margaria, M. Nicola, G. Povero, and M. T. Gamba, "N-FUELS and SOPRANO: Educational tools for simulation, analysis and processing of satellite navigation signals," in *Proc. IEEE Front. Educ. Conf. (FIE)*, Oklahoma City, OK, USA, 2013, pp. 303–308.

[22] J.-A. Ávila-Rodríguez, "On generalized signal waveforms for satellite navigation," M.S. thesis, Dept. Faculty Aerosp. Eng., Univ. FAF Munich, Munich, Germany, 2008.

[23] *NAVSTAR GPS Space Segment/Navigation User Segment Interfaces (IS-GPS-200)*, U.S. Air Force, Washington, DC, USA, 2020.

[24] *Galileo Open Service, Signal in Space Interface Control Document (OS SIS ICD V1.3)*, Eur. Union, Brussels, Belgium, 2016.

[25] A. Joseph and M. Petovello, *Measuring GNSS Signal Strength*, vol. 5, Inside GNSS, Red Bank, NJ, USA, 2010, pp. 20–25.
[26] J. J. Spilker Jr., P. Axelrad, B. W. Parkinson, and P. Enge, *Global Positioning System: Theory and Applications, Volume I*. Washington, DC, USA: Amer. Inst. Aeronaut. Astronaut., 1996.

Andrea Nardin (Student Member, IEEE) received the M.Sc. degree in telecommunications engineering from the Politecnico di Torino, with a thesis on collaborative GNSS ranging integration in positioning algorithms, where he is currently pursuing the Ph.D. degree with the Department of Electronics and Telecommunications within the Navigation Signal Analysis and Simulation Research Group. His work is focused on innovative signal processing architectures and signal design for GNSS.

Fabio Dovis (Member, IEEE) was born in Bruino, Italy, in 1970. He received the M.Sc. and Ph.D. degrees from the Politecnico di Torino, Turin, Italy, in 1996 and 2000, respectively. He joined the Department of Electronics and Telecommunications, Politecnico di Torino as an Assistant Professor in 2004, and since 2014, he has been an Associate Professor with the Department of Electronics and Telecommunications, where he coordinates the Navigation Signal Analysis and Simulation (NavSAS) Research Group. He has a relevant experience in European projects in satellite navigation as well as cooperation with industries and research institutions. His research interests cover the design of GPS and Galileo receivers and advanced signal processing for interference and multipath detection and mitigation, as well as ionospheric monitoring. He serves as a member of the IEEE Aerospace and Electronics Systems Society Navigation Systems Panel.

Juan A. Fraire (Senior Member, IEEE) is a Researcher with the Université de Lyon, Inria, INSA Lyon, CITI, Villeurbanne, France, an Assistant Researcher with the National Research Council of Argentina (CONICET), and an Associate Professor with the Universidad Nacional de Córdoba (UNC, FAMAF) and Saarland University, Germany. He participates in joint projects with NASA's Jet Propulsion Laboratory and the Argentinian Space Agency (CONAE) and collaborates with world-renowned space companies. He has coauthored more than 45 papers published in international journals and leading conferences, and has imprinted a novel networking vision in his *Delay-Tolerant Satellite Network* book. His research focuses on spaceborne networking and distributed applications enabled by state-of-the-art informatics techniques. He is the Founder and the Chair of the annual Space-Terrestrial Internetworking Workshop.